# Resonance-Based Optimized Buck LED Driver Using Unequal Turn Ratio Coupled Inductance

Reza Sangrody, Mobina Pouresmaeil, Mousa Marzband, *Senior Member, IEEE*, and Edris Pouresmaeil, *Senior Member, IEEE*

***Abstract*—Losses in light-emitting-diode (LED) driver cause increasing temperature and shorten their lifespan. Therefore, improving the efficiency of LED drivers not only saves energy but also is indispensable to increase their lifespan. In this article, a new LED driver topology is proposed to improve the performance of valley switching by decreasing the MOSFET switching losses. The proposed topology is designed in a way that the MOSFET works at the significantly lower switching and conduction losses in compared with conventional LED drivers. It elaborates how the proposed topology also improves the overall efficiency by decreasing power losses in other main elements of the driver, including inductance and diode. In addition, a new valley switching implementation is introduced for the new converter, which decreases the cost and dimension of the LED drivers. The experimental results confirm the high efficient operation of the proposed LED driver by reaching the efficiency up to 97% at a wide range of operating voltage.**

***Index Terms*—Buck light-emitting-diode (LED) driver, high efficient LED driver, low output voltage, valley switching.**

## I. Introduction

TODAY incandescent and fluorescent lamps are replaced by light-emitting-diode (LED) lamps due to their long lifespan, nonmercury content, high efficiency, and simple control. A lot of researches investigated different aspects of these lamps to increase their controllability, efficiency, lifespan, and performance. These lamps need a driver to supply constant voltage or current. Different converter topologies, such as buck, boost, buck–boost, and flyback, are used as LED driver. These converter uses pulsewidth modulation technique to control the output current and voltage; as a result, the output current has ripple and the lamp has flicker. In this view, some studies focused on mitigating the output current ripple and attenuating the flicker [1]–[3]. Most of converters use a diode bridge and an electrolytic capacitor to supply the LED lamp. Some researches tried to eliminate the input bridge using new control method and novel LED driver [4], [5]. However, using electrolytic capacitors at the input of these converter shorten their lifespan; therefore, some researches tried to improve the lifespan of LED lamp by eliminating these bulk capacitor [6]–[11]. Poor power factor is another problem of these lamps which causes using power factor correction (PFC) converter for LED driver. However, using PFC converter increase the overall cost of LED lamp. Thus, some studies attempted to overcome this drawback by combining PFC converter and LED driver in a single converter [12]–[15]. Although LED lamps have higher efficiency in compared with other lamps, power losses in LED drivers cause rising temperature, which results in shortening their lifespan. Therefore, thermal management and preventing power loss in LED drivers are indispensable to control their temperature and improving LED's efficiency [16]. These losses are mainly included losses in converter inductance, diodes, input bridge, and losses in the MOSFET switching and conduction [17]. Zero voltage switching (ZVS) and zero current switching (ZCS) are implemented using resonance phenomena to decrease the switching losses and increase the efficiency [18]–[24]. However, extra circuit elements, such as capacitors and inductors, are required to implement the resonance which increases the size and overall cost issues. Valley switching method is a solution for these issues which uses the resonance between the converter inductance and parasitic output capacitance of the MOSFET instead of extra circuit elements [25]–[28]. However, the minimum point of resonance voltage is not low enough to decrease the switching losses sufficiently in low output voltage; therefore, using resonance in this condition is not efficient. In this article, a new topology is proposed to minimize the valley point of resonance at the MOSFET output voltage to zero, so that the MOSFET switching losses minimized at this point. Also, it shows that the new topology decreases the conduction losses of the MOSFET in addition to switching losses. Besides decreasing the MOSFET losses, the other elements' losses, such as inductor and diode conduction losses and input bridge losses, are decreased significantly. In this proposed topology, the implementation of valley switching without requiring a secondary winding makes an LED driver more efficient and cheaper in compared with other designs in which a secondary winding coupled by the converter inductance is required to detect the minimum point of the MOSFET output voltage [27]. Accordingly, the contributions of this article can be summarized as follows.

1) A new high efficient buck LED driver is introduced and its output current and voltage relation to the input reference

Manuscript received December 22, 2019; revised February 27, 2020; accepted April 20, 2020. Date of publication April 26, 2020; date of current version July 31, 2020. Recommended for publication by Associate Editor H.-K. Chen. *(Corresponding author: Reza Sangrody.)*

Reza Sangrody is with the Department of Electrical and Computer Engineering, Firoozkooh Branch, Islamic Azad University, Firoozkooh 47137-57768, Iran (e-mail: sangrody@iaufb.ac.ir).

Mobina Pouresmaeil and Edris Pouresmaeil are with the Department of Electrical Engineering and Automation, Aalto University, 02150 Espoo, Finland (e-mail: mobina.pouresmaeil@aalto.fi; edris.pouresmaeil@aalto.fi).

Mousa Marzband is with the Department of Mathematics, Physics and Electrical Engineering, Northumbria University, Newcastle upon Tyne NE1 8ST, U.K. (e-mail: mousa.marzband@northumbria.ac.uk).

Color versions of one or more of the figures in this article are available online at https://ieeexplore.ieee.org.

Digital Object Identifier 10.1109/TPEL.2020.2990492

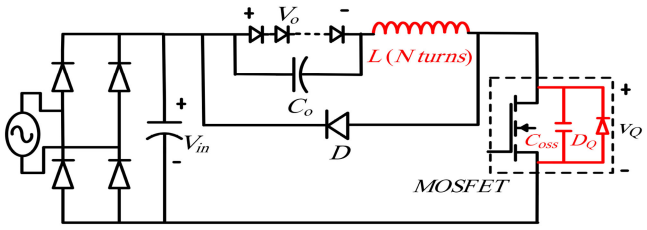


Fig. 1. Conventional buck LED driver.

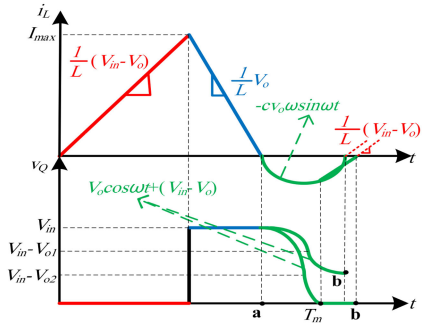


Fig. 2. Inductance current and the MOSFET output voltage (red, blue, and green colors are signals related to the ON state switching, OFF state switching, and resonance, respectively).

current and input voltage is achieved. In addition, all main element losses analyzed and illustrated by equations and figures.

2) A new valley switching is introduced according to the new topology, which is implemented more easily and cost effective.

The rest of the article is organized as follows. In Section II, valley switching in buck LED drivers is explained. Section III elaborates the operation of the proposed LED driver while in Section IV the efficiency of the proposed topology is compared with the conventional buck LED driver. In Section V, the implementation of new valley switching is represented. The experimental results of the proposed topology are shown in Section VI. Finally, the conclusions is drawn in Section VII.

## II. Valley Switching in Buck LED Drivers

Fig. 1 shows conventional buck LED driver in which the MOSFET is placed in the low voltage side. Valley switching method uses resonance between converter inductance ($L$) and parasitic output capacitance of MOSFET ($C_{oss}$) to decrease the switching losses. The MOSFET output capacitance and its body diode and the converter inductance are shown in red color to emphasis the main resonance elements. Fig. 2 shows the inductance current and the MOSFET output voltage in current control mode and valley switching control. As can be seen, the inductance current rises to maximum reference current ($I_{\max}$) when the MOSFET turns ON, and then the MOSFET turns OFF and the inductance current falls to zero. A resonance is occurred at this moment between the converter inductance and parasitic output capacitance of the MOSFET (point **a**). The MOSFET turns

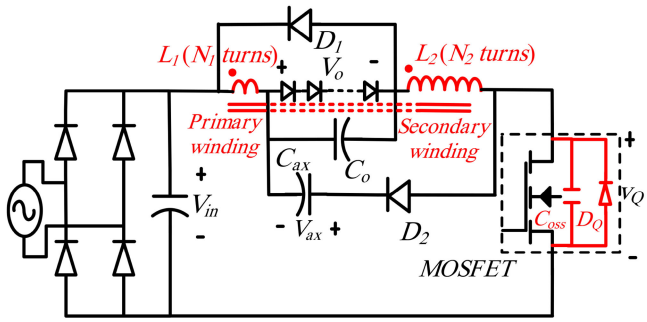


Fig. 3. Propose buck LED driver.

ON when the output voltage of the MOSFET reaches its minimum value or zero (point **b**). The output voltage equation of the MOSFET ($v_Q$) and the inductance current depend on input voltage value ($V_{\text{in}}$) and output voltage value ($V_o$). There are two cases. A full resonance oscillation is occurred when the input voltage value is greater than $2V_o$ while in the other case, the output voltage of MOSFET tends to be a negative value at $T_m$; therefore, the body diode of the MOSFET turns ON and output voltage clamps to zero. Equation (1) shows the output voltage of the MOSFET ($v_Q(t)$) for these two cases where the resonant angular frequency ($\omega$) is represented by (2)

$$v_Q(t) = \begin{cases} \begin{cases} (V_{\text{in}} - V_o) + V_o \cos(\omega t) & t \le T_m \\ 0 & t > T_m \end{cases} & V_{\text{in}} < 2V_o \\ (V_{\text{in}} - V_o) + V_o \cos(\omega t) & V_{\text{in}} \ge 2V_o \end{cases} \tag{1}$$

$$\omega = \frac{1}{\sqrt{LC_{oss}}}. \tag{2}$$

The output voltage of the conventional converter can be achieved by inductance volt-second method

$$V_o = D_{CC} V_{\text{in}} \tag{3}$$

where $D_{CC}$ is duty cycle of the conventional converter. The ON state switching losses depend on input voltage and output voltage values as shown in the following:

$$P_{sw\text{ON}} = \begin{cases} 0.5 f_{sw} C_{oss} (V_{\text{in}} - 2V_o)^2 & V_{\text{in}} \ge 2V_o \\ 0 & V_{\text{in}} < 2V_o \end{cases} \tag{4}$$

where $P_{sw\text{on}}$ and $f_{sw}$ are ON state switching losses and switching frequency, respectively. Equation (4) indicates that switching losses increase in applications where the output voltage value is low.

## III. Operation of the Proposed LED Driver

Minimum value of the MOSFET's voltage is $(V_{\text{in}} - 2V_o)$ according to (1); therefore, the switching losses increase in low output voltage, consequently the valley switching is not efficient for this application. Fig. 3 shows the proposed buck LED driver to overcome the high switching losses in low output voltage. In this converter, ZVS is achieved together with ZCS when valley

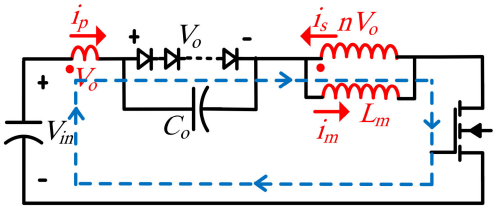


Fig. 4. Proposed circuit in MOSFET ON state.

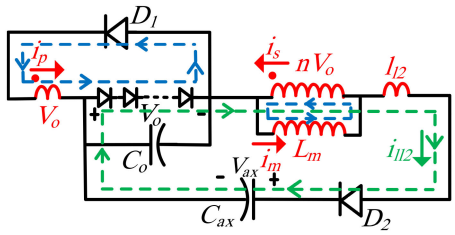


Fig. 5. Proposed circuit in MOSFET OFF state.

switching is activated. Here, in this configuration, the converter inductance ($L$), previously shown in Fig. 1 with $N$ turns, is divided into two inductances with $N_1$ and $N_2$ turns, which are wound on a core to build coupled windings ($N = N_1 + N_2$). As shown in (5), the winding turn ratio ($n$) of these inductances is equal or greater than the ratio of input voltage to output voltage values subtracted by 2

$$n = \frac{N_2}{N_1} \geq \left( \frac{V_{\text{in}}}{V_o} - 2 \right). \tag{5}$$

Note that the secondary winding turns are higher than the primary turns and, as shown in Fig. 3, an auxiliary capacitor ($C_{ax}$) and a diode ($D_2$) are connected to it. In this configuration, the secondary voltage becomes equal to the output voltage value ($V_o$) in OFF state of the MOSFET if this capacitor is emitted; therefore, the primary voltage value becomes lower than the output voltage. In this condition, the diode $D_1$ is backward biased and it never turns ON. This capacitor prevents diode $D_2$ from conducting in OFF state of the MOSFET.

The reason is that since there is not any load parallel to $C_2$, its average current is not zero and its voltage becomes greater than $nV_o$ and in this moment the $D_2$ becomes backward biased, therefore only diode $D_1$ conducts when the MOSFET turns OFF. Fig. 4 shows the driver when the MOSFET is in ON state. In this figure, the transformer model of coupling inductance is used. Note that because leakage inductances do not affect the circuit operation, they are not shown for simplicity in illustration. Similarly, diodes $D_1$ and $D_2$ are backward biased in this state; therefore, they are not included in this figure. Primary current of transformer is the load current of the converter which can calculated by (6) where $i_p$, $i_s$, and $i_m$ are the primary, secondary, and magnetizing current of the transformer, respectively.

$$\left.\begin{aligned} & i_p = n i_s \\ & i_m = i_s + i_p = \tfrac{n+1}{n} i_p \\ & v_{Lm} = \tfrac{n}{n+1} \left( V_{\text{in}} - V_o \right) \end{aligned}\right\} => i_p(t)$$

$$= \frac{1}{L_m} \left( \frac{n}{n+1} \right)^2 \left( V_{\text{in}} - V_o \right) \, t \tag{6}$$

where $L_m$ is the magnetizing inductance of the transformer. In current control mode, the MOSFET turns OFF when the output current reaches to a predetermined maximum reference value ($I_{NC\max}$). Fig. 5 shows transformer model of inductance and emits elements which do not affect the operation when the MOSFET is in OFF state. In steady state, when the MOSFET turns OFF, only diode $D_1$ conducts and resets the magnetizing inductance

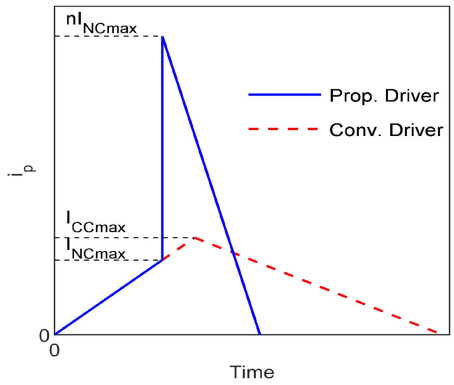


Fig. 6. Theoretical waveform of inductance current for the conventional and the proposed converter.

energy and diode $D_2$ does not conduct. In real application and nonideal inductance, diode $D_2$ discharges the leakage inductance energy of secondary winding ($l_{l2}$). The output current can be calculated by

$$\left.\begin{aligned} & i_p = n i_s \\ & i_m = i_s = \tfrac{1}{n} i_p \\ & v_{Lm} = -n V_o \\ & i_m = I_{NC\max} + \tfrac{1}{L_m} V_{Lm} t \end{aligned}\right\} => i_p(t)$$

$$= n I_{NC\max} - \frac{1}{L_m} n^2 V_o \, t. \tag{7}$$

Fig. 6 shows the output current of the proposed current according to (6) and (7). The average output current can be calculated using the primary current

$$I_{NCave} = \frac{1}{2} \left( D_{NC} + n \left( 1 - D_{NC} \right) \right) I_{NC\max} \tag{8}$$

where $I_{NCave}$ and $D_{NC}$ are average current and duty cycle of the proposed converter, respectively. This current for conventional converter is

$$I_{CCave} = \frac{1}{2} I_{CC\max} \tag{9}$$

where $I_{CCave}$, and $I_{CC\max}$ are, respectively, the average, and maximum current of the conventional converter. The steady state output voltage value (10) and auxiliary capacitors voltage value (11) can be calculated using voltage second of inductor

$$V_o = \frac{D_{NC}}{D_{NC} + (n+1)(1 - D_{NC})} V_{\text{in}} \tag{10}$$

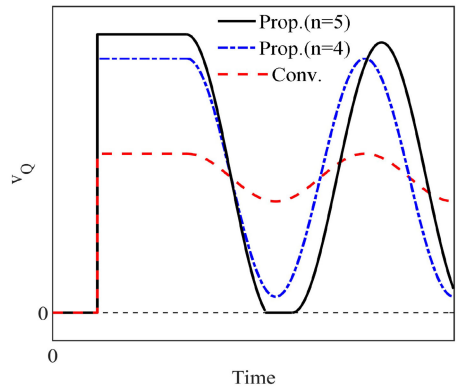


Fig. 7. Theoretical MOSFET output voltage for the conventional and the proposed converter.

$$V_{ax} = \frac{kD_{NC}}{D'}(V_{in} - V_o) + (n-1)V_o\,,\ k = \frac{l_{l2}}{L_{11} + L_{22} + 2L_{12}} \tag{11}$$

where $L_{11}$, $L_{22}$, and $L_{12}$ are the primary and secondary winding self and mutual inductances, respectively, and $l_{l2}$ represents the leakage inductance of the secondary winding.

*D'* shows the ratio of falling time of the leakage inductance current to switching period. Note that the leakage inductance value is very smaller than magnetizing inductance; therefore, the current caused by secondary leakage inductance is in discontinuous mode.

When the current reaches zero, a resonance is occurred through the circuit involving of input voltage ($V_{\rm in}$), windings ($N_1$ and $N_2$), output voltage ($V_o$), and the MOSFET output capacitance ($C_{oss}$). The MOSFET output voltage by neglecting the leakage inductance ($l_{l2}$) is calculated using (12)

$$v_Q(t) = (V_{\rm in} - V_o) + (n+1)V_o\cos(\omega t) \tag{12}$$

$$\omega = \frac{1}{\sqrt{L_{\rm eq}C_{oss}}},\ L_{\rm eq} = \left(\frac{n+1}{n}\right)^2 L_m. \tag{13}$$

Comparing (1) with (11) indicates that the minimum output voltage of the MOSFET decreases from $(V_{\rm in} - 2V_o)$ to $(V_{\rm in} - (n+2)V_o)$. This minimum value can be decreased to zero if (5) is regarded because the reverse body diode of the MOSFET conducts when this voltage tends to be negative. In this condition, ZVS will accompany ZCS if valley switching activates. Fig. 7 shows the MOSFET output voltage for the conventional and the proposed LED driver for typical elements' value, and for two ratio values of $n = 4$ and $n = 5$. As seen the minimum point of the MOSFET output voltage is zero when the turn ratio is greater than 4. In fact, in this condition, the reverse body diode of the MOSFET turns ON and the output voltage of the MOSFET is clamped to zero.

## IV. Efficiency Comparison

All losses consist of the MOSFET (both for ON and OFF switching losses), inductors and diodes conducting losses are investigated to compare the efficiency of the proposed driver with the conventional buck LED driver. The average output current of the proposed and conventional converters LED drivers should be equal to compare the conducting losses of inductors or diodes. The average output current of the proposed converter in (8) is equal to its value for the conventional in (9), if the following equation is satisfied:

$$I_{NC\max} = \frac{1}{(D_{NC} + n(1 - D_{NC}))} I_{CC\max}. \tag{14}$$

The rms values of output currents for both converters should be calculated as follows to compare the conduction losses:

$$I_{NCrms} = \frac{I_{NC\max}}{\sqrt{3}}\sqrt{D_{NC} + n^2(1 - D_{NC})} \tag{15}$$

$$I_{CCrms} = \frac{I_{CC\max}}{\sqrt{3}} \tag{16}$$

where $I_{NCrms}$ and $I_{CCrms}$ are the proposed and conventional converter output rms currents, respectively. The rms current value of the proposed LED driver can be achieved as a function of rms current value of the conventional LED driver using (14)–(16)

$$I_{NCrms} = I_{CCrms}\frac{\sqrt{D_{NC} + n^2(1 - D_{NC})}}{(D_{NC} + n(1 - D_{NC}))}. \tag{17}$$

If the output voltage of the conventional and the proposed converters becomes equal, the relationship between their duty cycle can be achieved by (3) and (10)

$$D_{CC} = \frac{D_{NC}}{D_{NC} + (n+1)(1 - D_{NC})}. \tag{18}$$

### A. MOSFET Switching Losses

While the OFF state switching losses are the same at two converters, they are different at the ON state switching loss. According to (4), the ON state switching loss of the MOSFET increases in low voltage applications in conventional converters but it is zero in the proposed LED driver.

### B. MOSFET Conduction Losses

Conduction losses depend on the MOSFET rms current and its ON state resistance ($R_{\rm on}$)

$$P_{NCMcon} = R_{\rm ON}\frac{I^2_{NC\max}}{3}D_{NC} \tag{19}$$

$$P_{CCMcon} = R_{\rm ON}\frac{I^2_{CC\max}}{3}D_{CC} \tag{20}$$

where $P_{NCMcon}$ and $P_{CCMcon}$ are the proposed and conventional MOSFET conduction losses of conventional converter, respectively. The MOSFET conduction loss can be compared using (14), (18)–(20)

$$P_{NCMcon} = M_{CMOS} \times P_{CCMcon}$$

$$M_{CMOS} = \frac{D_{NC} + (n+1)(1 - D_{NC})}{(D_{NC} + n(1 - D_{NC}))^2}. \tag{21}$$

Fig. 8 shows coefficient $M_{CMOS}$ versus duty cycle for different turn ratios. As seen, the conduction loss of the MOSFET

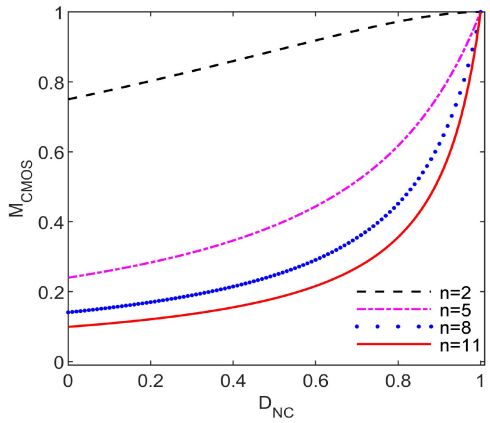


Fig. 8. Coefficient $M_{CMOS}$ versus duty cycle $(D_{NC})$ for different turn ratios.

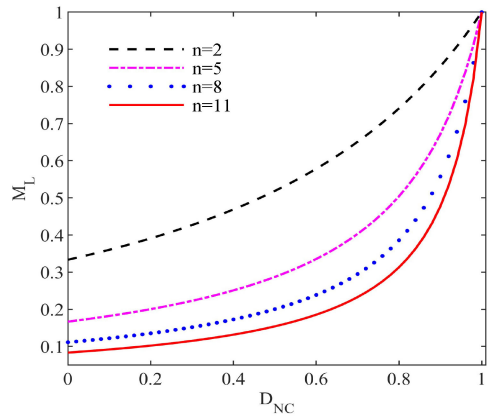


Fig. 9. Coefficient $M_L$ versus duty cycle $(D_{NC})$.

in new converter is lower than its value for the conventional converter because the coefficient is less than one for all rages of the duty cycle

### C. Inductors Conducting Losses

Resistance of the primary and secondary windings are represented in (22) and (23), respectively

$$R_p = \frac{1}{n+1} R_w \tag{22}$$

$$R_s = \frac{n}{n+1} R_w \tag{23}$$

where $R_p$, $R_s$, and $R_w$ are primary, secondary, and total windings resistance, respectively. Primary and secondary winding losses ($P_{priw}$ and $P_{\text{sec}w}$) can be calculated using these resistances and their rms current values

$$P_{priw} = \frac{1}{n+1} R_w \frac{I_{NC\max}^2}{3} \left(D_{NC} + n^2 \left(1 - D_{NC}\right)\right) \tag{24}$$

$$P_{\text{sec}\,w} = \frac{n}{n+1} R_w \frac{I_{NC\max}^2}{3} D_{NC}. \tag{25}$$

Inductor loss of the proposed and conventional LED driver can be calculated using (14)–(17), (24), and (25). It can be expressed as

$$P_{NCLL} = M_L \times P_{CCLL}$$

$$M_L = \frac{1}{n+1} \frac{D_{NC} + n^2 \left(1 - D_{NC}\right) + n D_{NC}}{\left(D_{NC} + n \left(1 - D_{NC}\right)\right)^2} \tag{26}$$

$$P_{CCLL} = R_w I_{CCrms}^2 \tag{27}$$

where $P_{NCLL}$ and $P_{CCLL}$ are inductor loss of the proposed and conventional converter, respectively. Fig. 9 shows coefficient $M_L$ for different turn ratios. As can be seen, $M_L$ is less than 1; therefore, inductor loss of the proposed converter is less than inductor loss of the conventional converter.

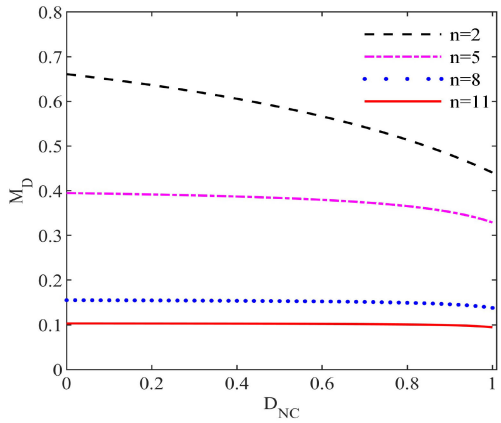


Fig. 10. Coefficient $M_D$ versus duty cycle $(D_{NC})$.

### D. Diodes Conducting Losses

As explained in the previous section, only diode $D_1$ turns ON when the MOSFET turns OFF. Diode loss depends on its forward voltage drop $(V_F)$ and its average current

$$P_{NCDL} = \frac{1}{2} I_{NC\max} V_F \left(1 - D_{NC}\right) \tag{28}$$

$$P_{CCDL} = \frac{1}{2} I_{CC\max} V_F \left(1 - D_{CC}\right) \tag{29}$$

where $P_{NCDL}$ and $P_{CCDL}$ are diode losses of the proposed and conventional converters, respectively. It is supposed that the forward voltage of the diode is constant for simplicity. Diode losses can be compared using (14), (18), (28), and (29)

$$P_{NCDL} = M_D \times P_{CCDL}$$

$$M_D = \frac{\left(D_{NC} + (n+1)\left(1 - D_{NC}\right)\right)}{(n+1)\left(D_{NC} + n\ \left(1 - D_{NC}\right)\right)}. \tag{30}$$

Fig. 10 shows coefficient $M_D$ for different turn ratios. It shows that the diode loss in the proposed LED driver is less than the conventional diode loss.

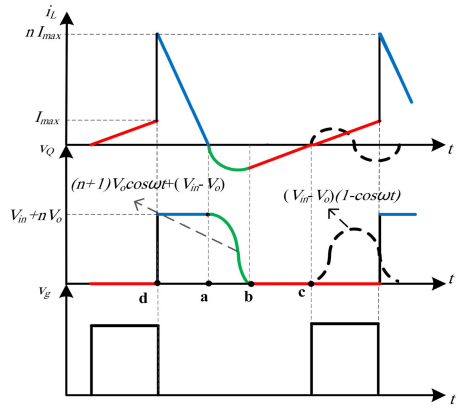


Fig. 11. Theoretical waveform of inductance current, the MOSFET output, and gate voltage.

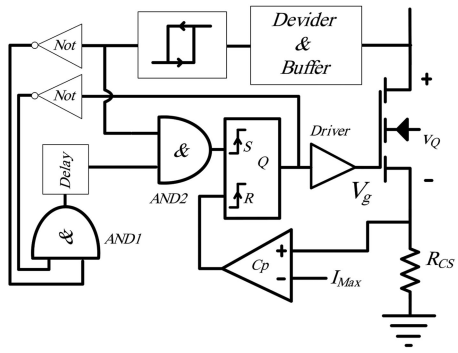


Fig. 12. New valley switching.

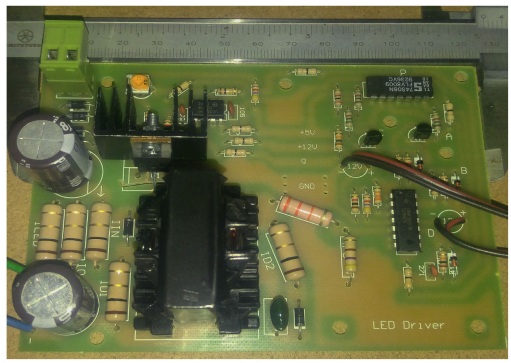


Fig. 13. Experimental setup.

## V. New Valley Switching Implementation

In the conventional LED drivers a secondary winding is coupled to the converter inductance to implement the valley switching. The minimum point of output voltage of the MOSFET occurs when the slope of voltage across this winding approaches zero. The extra winding causes cost and size of the converter increases. In addition, an extra sensing pin in controller IC is needed [27].

A new method to implement valley switching can be introduced using the proposed converter. Fig. 11 shows the inductance current, the MOSFET output voltage, and the MOSFET gate voltage. In current control mode, the gate pulse becomes zero when the inductance current reaches the reference maximum current ($I_{\max}$). The converter diodes conduct at point **d** after a resonance, which is not shown in this figure. Another resonance occurs between the inductor current and the MOSFET parasitic capacitance just the current reaches zero value and diodes turn OFF (point **a**). The reverse body diode of the MOSFET conducts just the output voltage of the MOSFET tends to be a negative value (point **b**); therefore, the inductance current rises from a negative value and the reverse diode turns OFF when this current becomes positive (point **c**). At this moment, a resonance occurs between the converter inductance and the parasitic output capacitance of the MOSFET

$$v_Q(t) = (V_{\text{in}} - V_o)(1 - \cos(\omega t)), \omega = \frac{1}{\sqrt{L_{\text{eq}} C_{oss}}}. \quad (31)$$

The next switching should be done at point **c** to implement the ZCS accompanied by ZVS. The main characteristic of point **c** is that it occurs when the MOSFET output voltage is zero while the gate pulse is zero too. The next switching point can be done by knowing this fact and should be done just the MOSFET voltage tends to be a positive value. Although the method is explained for zero drain-source voltage at points **b** and **c**, any drain-source voltage can be used instead of zero. This case occurs when the output voltage is very low and drain-source resonant voltage does not tend to be a negative value and the body diode of the MOSFET does not conduct. Fig. 12 shows the implementation of this switching method. The output of gate *AND1* goes high when both the MOSFET gate and output voltage become zero. This gate's output after a small delay provides the first input signal of gate *AND2*. This delay is due to preventing switching at point **d**. The output of this gate *AND2* becomes high just the MOSFET output voltage tends to be a positive value (point **c**). Consequently, the output of flip-flop becomes high and the MOSFET turns ON at this point.

Many converter IC controllers in current control mode have separated synchronizing pin or can do synchronization using oscillation pin. The output signal of *AND2* can be connected to synchronizing pin and the output signal of current comparator (*Cp*) can supply the current control pin of these ICs; therefore, the extra sensing pin is not required.

## VI. Experimental Results

Figs. 13 and 14 show the experimental setup used to implement the proposed LED driver. A 15 W/33 V LED lamp is used as output load and UC3844 converter controller is used in current control mode. This IC uses oscillation pin (pin 4) for synchronization. The current feedback is implemented by a resistor connected to the source pin of the MOSFET. Other specifications are shown in Table I.

The input and output voltage values are 310 and 33 V, respectively; therefore, the primary and secondary winding numbers are 27 and 166 turns, respectively. Fig. 15 shows the current waveform of the proposed and conventional converters when the valley switching is implemented. It verifies the theoretical

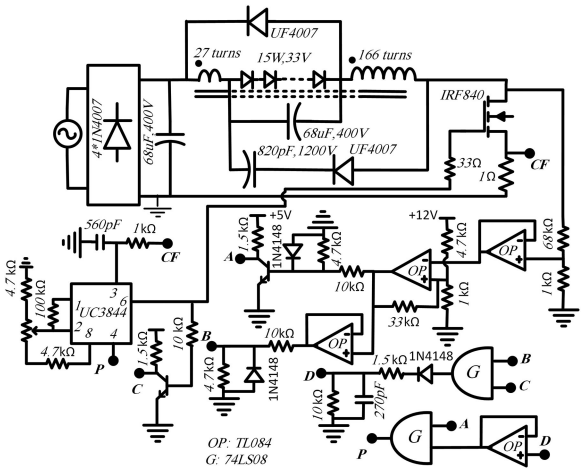


Fig. 14. LED driver circuit.

TABLE I
SYSTEM PARAMETERS

| Parameter | Description | Value |
|---|---|---|
| MOSFET | The main switch | IRF840 |
| IC Controller | Converter controller IC | UC3844 |
| $N_1$ | Primary winding | 27 |
| $N_2$ | Secondary winding | 166 |
| $C_o$ | Output capacitor | 68uF,400V |
| $C_{ax}$ | Auxiliary capacitor | 820PF,1200V |
| $C_{in}$ | Input capacitor | 68uF,400V |
| $D_1$ | Primary winding diode | UF4007 |
| $D_2$ | Secondary winding diode | UF4007 |
| $R_{cs}$ | Current feedback resistor | 1Ω,1W |
| $R_G$ | The MOSFET gate resistor | 33Ω,0.25W |

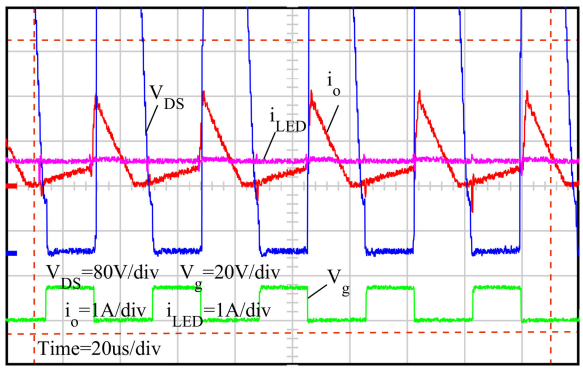


Fig. 15. Drain-source voltage of the MOSFET ($V_{DS}$), output current ($i_o = i_{Co} + i_{\rm LED}$), LED current ($i_{\rm LED}$), and gate-source voltage of the MOSFET ($V_g$).

waveform of Fig. 6 and there is no voltage oscillation because the ON switching state occurs at the minimum point of the MOSFET output voltage.

Valley switching can be disabled to show the MOSFET output voltage oscillations in the proposed LED driver. Fig. 16 shows the output voltage of the MOSFET for the proposed LED driver when the valley switching is not performed and the converter works in DCM mode. As seen, the minimum point of the output voltage approaches near zero in the proposed circuit, therefore

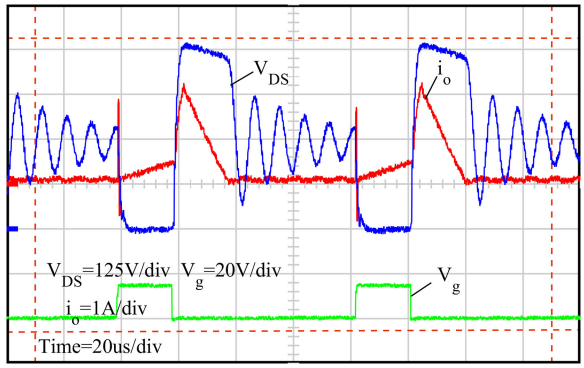


Fig. 16. Drain-source voltage of the MOSFET ($V_{DS}$), output current ($i_o$ i$_{\rm Co}$+$i_{LED}$>), and gate-source voltage of the MOSFET ($V_g$) for the proposed converter when valley switching is disabled ($V_{\rm in}$ = 310 V and $V_o$ = 33V).

TABLE II
WORKING CONDITION

| Parameter | Description | Value |
|---|---|---|
| $I_o$ | Output current | 450 mA |
| $I_{CCmax}$ | $I_{max}$ for the conventional LED driver | 900 mA |
| $I_{NCmax}$ | $I_{max}$ for the proposal LED driver | 241 mA |
| $D_{CC}$ | Duty cycle of the conventional LED driver | 0.105 |
| $D_{NC}$ | Duty cycle of proposal LED driver | 0.455 |

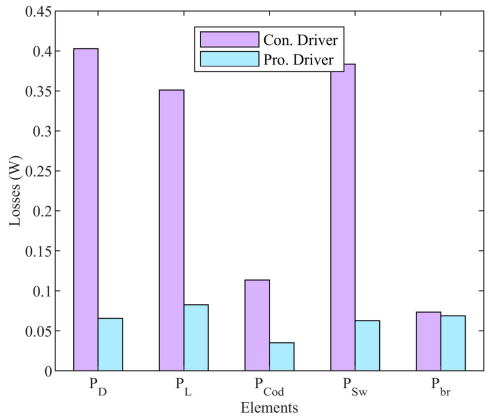


Fig. 17. Losses of converter elements. $P_D$: converter diodes losses, $P_L$: inductance losses, $P_{Cond}$: MOSFET conduction losses, $P_{Sw}$: MOSFET switching losses, and $P_{br}$: diode bridge losses.

if the valley switching is activated, the switching losses will be much smaller than the conventional converter.

The losses of LED driver elements including losses in inductance, diode, and the MOSFET for the proposed and conventional LED driver are calculated at the same working conditions using (3), (9), (14), and (18) are shown in Table II. Fig. 17 illustrates the losses of converter elements consist of inductance, diode, and the MOSFET for the proposed and conventional LED driver. It can be seen in this figure that the losses of the proposed circuit are much smaller than their values for the conventional LED driver.

In this condition, the efficiency of the proposed LED driver is 98%, whereas the efficiency of the conventional LED driver is 92%. Fig. 18 shows the efficiency of the proposed and conventional converters as a function of output voltage. The input

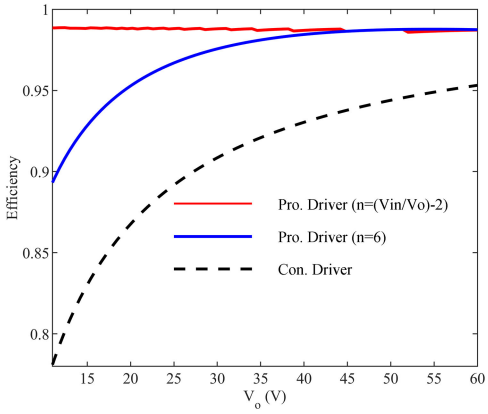


Fig. 18. Proposed and conventional converter efficiency.

TABLE III
COMPARISON OF THE PROPOSED LED DRIVER WITH [22]–[24]

| | [22] | [23] | [24] | Proposed LED Driver |
|---|---|---|---|---|
| MOSFET | 2 | 1 | 2 | 1 |
| Diode | 2 | 3 | 2 | 2 |
| Capacitor | 3 | 4 | 4 | 3 |
| Magnetic core | 1 | 2 | 2 | 1 |
| Efficiency at 15W output | 91% | 92% | 89% | 97% |

voltage values are set 310 V and the windings turn ratio is regarded 6 using (4).

As seen, the efficiency of the conventional LED driver is lower than the proposed LED driver for the range of output voltage. In addition, at lower range of output voltage, the difference between two LED drivers' efficacy is even more significantly. As an example, at output voltage equal to 10 V, the efficiency of the proposed LED driver is 97%, and 89% for turn ratio achieved by (5), and $n = 6$, respectively, while it is only 78% in the conventional converter.

The proposed LED driver was compared with some similar researches by number of devices and achieved efficiency. Table III shows the result. As seen, the efficiency of the proposed LED driver is higher than the previous similar researches. Also, the proposed LED driver required one MOSFET, one magnetic core, two diodes, and three capacitors while the previous researches required more devices, which make the proposed LED drive more cheaper.

## VII. CONCLUSION

In this article, a new buck LED driver is introduced to improve its efficiency. By elaborating the proposed driver configuration and analyzing power losses of main elements (i.e., the MOSFET, inductors, and diodes) it is shown that at the same operating conditions, the proposed LED driver has much more higher efficiency than the conventional one. The reason is based on two principles. First, the minimum point of output resonant voltage of the MOSFET is near zero in the proposed LED driver; therefore, the switching loss of the MOSFET decreases dramatically using valley switching method. This result is more prominent when the output voltage value is very lower than the input voltage value. Second, the current waveform of the proposed LED driver is changed in a way that the other main losses consist of the MOSFET, inductance, and diode conduction losses are reduces strongly. Also, a new valley switching method is introduced according to the new converter, which does not require the coupling winding. Therefore, the cost and dimension of the proposed converter is much less than the conventional driver.

## REFERENCES

[1] X. Liu, X. Li, Q. Zhou, and J. Xu, "Flicker-free single switch multi-string LED driver with high power factor and current balancing," *IEEE Trans. Power Electron.*, vol. 34, no. 7, pp. 6747–6759, Jul. 2019.
[2] X. Liu, X. Li, Q. Zhou, and J. Xu, "Flicker-free single switch quadratic boost LED driver compatible with electronic transformers," *IEEE Trans. Ind. Electron.*, vol. 66, no. 5, pp. 3452–3467, May 2019.
[3] S. W. Lee and H. L. Do, "Boost integrated two-switch forward AC–DC LED driver with high power factor and ripple-free output inductor current," *IEEE Trans. Ind. Electron.*, vol. 64, no. 7, pp. 5789–5796, Jul. 2017.
[4] S. W. Lee and H. L. Do, "A single-switch AC-DC LED driver based on a boost-flyback PFC converter with lossless snubber," *IEEE Trans. Power Electron.*, vol. 32, no. 2, pp. 1375–1384, Feb. 2017.
[5] H. Ma, J. S. Lai, C. Zheng, and P. Sun, "A high-efficiency quasi-single-stage bridgeless electrolytic capacitor-free high-power AC–DC driver for supplying multiple LED strings in parallel," *IEEE Trans. Power Electron.*, vol. 31, no. 8, pp. 5825–5836, Aug. 2016.
[6] J. Liu, H. Tian, G. Liang, and J. Zeng, "A bridgeless electrolytic capacitor-free LED driver based on series-resonant converter with constant frequency control," *IEEE Trans. Power Electron.*, vol. 34, no. 3, pp. 2712–2725, Mar. 2019.
[7] P. Fang, S. Webb, Y. F. Liu, and P. C. Sen, "Single-stage LED driver achieves electrolytic capacitor-less and flicker-free operation with unidirectional current compensator," *IEEE Trans. Power Electron.*, vol. 34, no. 7, pp. 6760–6776, Jul. 2019.
[8] D. Gacio, J. M. Alonso, J. Garcia, D. G. Llera, and J. Gardesin, "Optimization of a front-end DCM buck PFP for an HPF integrated single-stage LED Driver," *IEEE J. Emerg. Sel. Topics Power Electron.*, vol. 3, no. 3, pp. 666–678, Sep. 2015.
[9] C. Shin *et al.*, "A sine-reference band (SRB)-controlled average current technique for a phase-cut dimmable AC–DC buck LED driver without an electrolytic capacitor," *IEEE Trans. Power Electron*, vol. 33, no. 8, pp. 6994–7009, Aug. 2018.
[10] P. S. Almeida, H. A. C. Braga, M. A. D. Costa, and J. M. Alonso, "Off-line soft-switched LED driver based on an integrated bridgeless boost–asymmetrical half-bridge converter," *IEEE Trans. Ind. Appl.*, vol. 51, no. 1, pp. 761–769, Jan. 2015.
[11] U. R. Reddy and B. L. Narasimharaju, "Single-stage electrolytic capacitor less non-inverting buck–boost PFC based AC–DC ripple free LED driver," *IET Power Electron.*, vol. 10, no. 1, pp. 38–46, Jan. 2017.
[12] Y. Hu, L. Huber, and M. M. Jovanovic, "Single-stage, universal-input AC/DC LED driver with current-controlled variable PFC boost inductor," *IEEE Trans. Power Electron.*, vol. 27, no. 3, pp. 1579–1588, Mar. 2012.
[13] A. Malschitzky, F. Albuquerque, E. A. Junior, and C. B. Nascimento, "Single-stage integrated bridgeless-boost nonresonant half-bridge converter for LED driver applications," *IEEE Trans. Ind. Electron.*, vol. 65, no. 5, pp. 3866–3878, May 2018.
[14] J. Baek and S. Chae, "Single-stage buck-derived LED driver with improved efficiency and power factor using current path control switches," *IEEE Trans. Ind. Electron.*, vol. 64, no. 10, pp. 7852–7861, Oct. 2017.
[15] L. Wang, B. Zhang, and D. Qiu, "A novel valley-fill single-stage boost-forward converter with optimized performance in universal-line range for dimmable LED lighting," *IEEE Trans. Ind. Electron.*, vol. 64, no. 4, pp. 2770–2778, Apr. 2017.
[16] X. Perpina *et al.*, "Thermal management strategies for low and high voltage retrofit LED lamp drivers," *IEEE Trans. Power Electron.*, vol. 34, no. 4, pp. 3677–3688. Apr. 2019.
[17] G. Z. Abdelmessih, J. M. Alonso, and M. A. D. Costa, "Loss analysis for efficiency improvement of the integrated buck-flyback LED driver," *IEEE Trans. Ind. Appl.*, vol. 54, no. 6, pp. 6543–6553, Nov. 2018.
[18] Y. Wang, X. Hu, Y. Guan, and D. Xu, "A single-stage LED driver based on half-bridge CLCL resonant converter and buck–boost circuit," *IEEE J. Emerg. Sel. Topics Power Electron.*, vol. 7, no. 1, pp. 196–208, Mar. 2019.

[19] Y. Wang, Y. Guan, J. Huang, W. Wang, and D. Xu, "A single-stage LED driver based on interleaved buck–boost circuit and LLC resonant converter," *IEEE J. Emerg. Sel. Topics Power Electron.*, vol. 3, no. 3, pp. 732–741, Sep. 2015.

[20] T. N. Gucin, B. Fincan, and M. Biberoglu, "A series resonant converter based multi-channel LED driver with inherent current balancing and dimming capability," *IEEE Trans. Power Electron.*, vol. 34, no. 3, pp. 2693–2703, Mar. 2019.

[21] X. Liu, Q. Zhou, J. Xu, Y. Lei, P. Wang, and Y. Zhu, "High-efficiency resonant LED backlight driver with passive current balancing and dimming," *IEEE Trans. Ind. Electron.*, vol. 65, no. 7, pp. 5476–5486, Jul. 2018.

[22] F. Pouladi, H. Farzanehfard, and E. Adib, "Battery operated soft switching resonant buck–boost LED driver with single magnetic element," *IEEE Trans. Power Electron.*, vol. 34, no. 3, pp. 2704–2711, Mar. 2019.

[23] S. W. Lee, H. J. Choe, and J. J. Yun, "Performance Improvement of a boost LED driver with high voltage gain for edge-lit LED backlights," *IEEE Trans. Circuits Syst. II, Exp. Briefs.* vol. 65, no. 4, pp. 481–485, Apr. 2018.

[24] Y. Wang, S. Goa, S. Zhang, and D. Xu, "A two-stage quasi-resonant dual-buck LED driver with digital control method," *IEEE Trans. Ind. Appl.*, vol. 54, no. 1, pp. 787–795, Jan. 2018.

[25] L. Huber, B. T. Irving, and M. M. Jovanpvic, "Effect of valley switching and switching-frequency limitation on line-current distortions of DCM/CCM boundary boost PFC converters," *IEEE Trans. Power Electron.*, vol. 24, no. 2, pp. 339–347, Feb. 2009.

[26] S. W. Lee and H. L. Do, "Single-stage bridgeless AC–DC PFC converter using a lossless passive snubber and valley switching," *IEEE Trans. Ind. Electron.*, vol. 63, no. 10, pp. 6055–6063, Oct. 2016.

[27] Y. C. Li, "A novel control scheme of quasi-resonant valley-switching for high-power-factor AC-to-DC LED driver," *IEEE Trans. Ind. Electron.*, vol. 62, no. 8, pp. 4787–4794, Aug. 2015.

[28] J. M. Wang and S. T. Wu, "A synchronous buck DC-DC converter using a novel dual-mode control scheme to improve efficiency," *IEEE Trans. Power Electron.*, vol. 32, no. 9, pp. 6983–6993, Sep. 2017.